Available online at www.sciencedirect.com

ScienceDirect

Advances in Space Research 73 (2024) 1050–1063

ADVANCES IN SPACE RESEARCH (a COSPAR publication)

www.elsevier.com/locate/asr

Empirical forecasting models for peak intensities of energetic storm particles at 1 AU

Dheyaa Ameri [a,b,*], Rami Vainio [b], Eino Valtonen [b]

[a] Department of Ecology, University of Basrah, Karmat Ali B.P. 49, Basrah, Iraq
[b] Department of Physics and Astronomy, University of Turku, 20014 Turku, Finland

Received 5 July 2023; received in revised form 10 October 2023; accepted 14 November 2023
Available online 20 November 2023

Abstract

We have investigated the dependence of the peak intensities of energetic storm particles (ESPs) on various parameters characterising the coronal mass ejections (CMEs) and associated phenomena. The aim of this study is to suggest empirical models for forecasting the peak intensities of ESP events at 1 AU based on solar and interplanetary (IP) space observations.

For this study we searched for the associations of front-side full and partial halo CMEs with linear speeds >400 km s^{-1}during the years 1996–2015 with IP shocks at 1 AU and ESP events observed near the time when the shock passes the observer. We found 88 CME-driven IP shocks associated with ESP events at proton energy range 5.0–7.2 MeV (nominal energy 6.0 MeV) and 59 shocks at the energy range 15.1–21.9 MeV (nominal energy 18.2 MeV). At these two energies 71% and 68% of the ESP events were associated with solar energetic particle (SEP) events, 85% and 84% were associated with decametric–hectometric (DH) type II radio bursts while 67% and 66% were associated with both.

For each CME - shock pair we calculated the predicted shock transit speed (V_{TR}) by using the method of Belov et al. (2022) and used this as the primary parameter in the investigation. We performed correlation analyses between the logarithm of the peak intensities of the ESP events ($\log_{10}$ [I_{ESP}^{peak}]) and the solar parameters related to the CMEs, solar flares, IP shocks, SEP events, and type II radio bursts. When using a single explanatory variable, we found best correlation coefficients for V_{TR}(0.68 ±0.05 and 0.71 ±0.06), the CME space speed (V_{CME}^{space}) (0.59 ± 0.05 and 0.68 ± 0.07), and the logarithm of SEP peak intensity ($\log_{10}$ [I_{SEP}^{peak}]) (0.55 ± 0.08 and 0.70 ±0.08) at 6.0 and 18.2 MeV, respectively. Weak to moderate correlations were found for the logarithm of the soft X-ray flux ($\log_{10}$ [SXRF]) and the logarithm of the duration of DH type II radio burst ($\log_{10}$ [D_{TII}]).

Using linear combinations of two or more variables improved the correlations. The best two-variable combination explaining $\log_{10}$ [I_{ESP}^{peak}] was V_{TR}combined with $\log_{10}$ [I_{SEP}^{peak}] and the best three- and four-variable combinations also included these two parameters. We found two methods for forecasting ESP peak intensities, one of which can be used for long lead time and the other for medium lead time forecasting. For long lead time forecasting V_{TR}, $V_{CME}^{space}$and $\log_{10}$ [SXRF] are used. The correlation coefficients between the calculated and observed $\log_{10}$ [I_{ESP}^{peak}] were 0.71 ±0.05 at 6.0 MeV and 0.74 ±0.06 at 18.2 MeV. This method only depends on the coronagraph and X-ray observations at the Sun. For medium lead time forecasting the four parameters used are V_{TR}, $\log_{10}$ [I_{SEP}^{peak}], V_{CME}^{space}(or $\log_{10}$ [SXRF]), and $\log_{10}$ [D_{TII}]. The correlation coefficients were 0.80 ±0.04 at 6.0 MeV and 0.84 ±0.05 at 18.2 MeV. Coronagraph observations at the Sun and solar energetic particle and DH type II burst measurements in IP space are required for this method. The medium lead time forecasting provides an average warning time of 30 ±16 h.

Keywords: Energetic particles; Solar particles; Energetic storm particles; Coronal mass ejections; Type II radio bursts; Interplanetary shocks

* Corresponding author at: Department of Ecology, University of Basrah, Karmat Ali B.P. 49, Basrah, Iraq.
E-mail addresses: dheyaa.abdulsada@uobasrah.edu.iq (D. Ameri), rami.vainio@utu.fi (R. Vainio), eino.valtonen@utu.fi (E. Valtonen).

https://doi.org/10.1016/j.asr.2023.11.021
0273-1177/© 2023 COSPAR. Published by Elsevier B.V.

1. Introduction

Energetic storm particle (ESP) events are defined as enhancements in energetic ion and electron intensities observed during an interplanetary shock passage (Bryant et al., 1962; Rao et al., 1967). The interplanetary shocks are primarily driven by coronal mass ejections (CMEs) and their interplanetary counterparts (ICMEs) (e.g., Lindsay et al., 1994; Berdichevsky et al., 2000) and sometimes by stream interaction regions (e.g., Jian et al., 2006, and references therein).

High-energy ESP events are an important constituent of space weather effects. Occurrence of ESP events can cause sudden, orders of magnitude increases of particle intensities near the Earth (see, e.g., Reames, 1999; Reames, 2004; Turner, 2001; Cohen, 2006). Temporal changes in near-Earth radiation environment can be a major concern due to the serious effects on the presence of humans in space and the operation of spacecraft and satellites (Cohen, 2006). Our goal is to find forecasting models for the peak intensities of ESP events by using parameters observed at the Sun and in IP space.

Many studies have investigated the occurrence and particle fluxes of ESP events and their dependences on the solar sources and shock parameters by using different samples of events. ESP events observed at a few tens of keV to a few MeV proton energies have been found to be associated with ∼32% – ∼80% of the shocks and with ∼20% – ∼40% of the shocks at electron energies of a few tens of keV (Ho et al., 2008; Huttunen-Heikinmaa and Valtonen, 2009; Mäkelä et al., 2011; Dierckxsens et al., 2015; Ameri et al., 2023). The characteristics of CMEs (CME speed) and interplanetary shocks (shock speed, Alfvénic Mach number, and compression ratio) associated with an ESP event have also been found to be more energetic compared to those without an ESP event. The ESP events occur more frequently and have higher intensities in the CME-driven shocks with type II radio bursts and SEP events compared to CME-driven shocks without those associations (e.g., Luhmann and Mann, 2007; Mäkelä et al., 2011; Giacalone, 2012; Ameri et al., 2023). Luhmann and Mann (2007) found a strong correlation between the ESP peak intensity and the related SEP peak intensity at 1 and 10 MeV proton energies. They suggested to use the peak intensity of the SEP events for estimating the peak intensity of the ESP events. Wijsen et al. (2022) used an energetic particle acceleration and transport model together with a solar wind and CME model to simulate the ESP event of 14 July 2012. They found that the simulation results agree well with both the upstream and downstream components of the ESP event for energies below 1 MeV observed by the Advanced Composition Explorer.

The proton peak intensities of ESP events have shown good to moderate correlations with CME speeds at the Sun (0.37 – 0.69), and shock speeds (0.44 – 0.70) and Alfvénic Mach number (0.26 – 0.59) at 1 AU (Mäkelä et al., 2011; Ameri et al., 2023). Ameri et al. (2023) found the highest correlations of the ESP peak intensities at different particle energies with the observed shock transit speed. Frequent association of ESP events with shocks producing DH type II radio bursts (e.g., Ameri et al., 2023) indicate that shocks can continuously accelerate electrons until reaching Earth. Ameri et al. (2023) concluded that the occurrence rate of ESP events and the correlations of the ESP peak intensities with CME and IP shock parameters were energy dependent. They found the highest correlation of the ESP peak intensity with the observed shock transit speed. This implies that shocks with high transit speeds often maintain their strength up till 1 AU and are capable to accelerate, not only electrons, but also protons which are observed as ESPs.

In this article, we investigate the dependence of the peak intensities of ESP events at two energy ranges (5.0–7.2 MeV and 15.1–21.9 MeV) on the characteristics of their solar sources and associated phenomena at the Sun and in IP space. In Section 2 we describe the data sources and event selection. The statistics of the events and the correlation analyses using single and multiple explanatory variables with a brief discussion of the lead time of the suggested ESP forecasting methods are presented in Section 3. The main results are summarised and discussed in Section 4, and the conclusions are presented in Section 5.

2. Data sources and event selection

The CME catalog of the SOHO Large Angle Spectroscopic Coronagraph (LASCO) (Brueckner et al., 1995) at https://cdaw.gsfc.nasa.gov/CME_list/ was used to select the CMEs. To identify the solar locations of the CMEs we assume the CME launch sites to coincide with the locations of the associated GOES soft X-ray flares given at https://ngdc.noaa.gov/stp/space-weather/solar-data/solar-features/solar-flares/x-rays/goes/xrs/. For this investigation we selected full and partial (angular width >120°) halo CMEs with speeds >400 $\mathrm{km\,s^{-1}}$launched from the front side of the Sun during the period from the beginning of 1996 to the end of 2015. When selecting the events, we used the widths and linear speeds given in the LASCO CME catalog.

The occurrence times of the IP shocks that we associated with the selected CMEs were obtained from the online IP shock database of the Wind and ACE spacecraft (https://lweb.cfa.harvard.edu/shocks/ and http://www.ssg.sr.unh.edu/mag/ace/ACElists/obs_list.html). We used the catalog compiled by Gopalswamy et al. (2019) available online at https://cdaw.gsfc.nasa.gov/CME_list/radio/waves_type2.html to associate DH type II radio bursts with the events.

To associate CMEs with IP shocks we followed the procedures presented in Ameri et al. (2023), where the drag-based model (Vršnak et al., 2013) was used to identify the definite CME-shock pairs (for more details see Section 2 of Ameri et al., 2023). The list of CME-driven shocks observed at 1 AU from Gopalswamy et al. (2010), the online catalog of SOHO/CELIAS (https://space.umd.

edu/pm/) and the recent list of CMEs and ICMEs provided by Belov et al. (2022) were used to assist associating CMEs with IP shocks at 1 AU.

For searching the energetic particle events related to the CME-driven shocks we used the European Space Agency (ESA) Solar Energetic Particle Environment Modelling (SEPEM) database (http://www.sepem.eu/) (Crosby et al., 2015). For details about the features of the SEPEM server see Crosby et al. (2015). The SEPEM Reference Data Set (version 2.01) has eleven energy channels extending from 5.0–7.2 MeV (nominal energy 6.0 MeV) to 200–289 MeV (240 MeV). The nominal energies are calculated as the geometric mean of the upper (E_{max}) and lower (E_{min}) limits of the energy channels ($E_{nominal} = \sqrt{E_{min} \cdot E_{max}}$). We define an ESP event as an increase of particle intensity at the shock passage at least 20% above the observed background intensity. The ESP peak intensity often occurred within a ±2 h time window from the observed shock time. The background intensity was estimated during a time period before the start of the ESP event (see, e.g., Mäkelä et al., 2011; Reames, 2012). Most of the ESP events were preceded by SEP events. To record an SEP event, the particle intensity should increase by a factor of 3 above the pre-event background intensity within a few hours (<3 h) after the launch of the CME (see, e.g., Kouloumvakos et al., 2015).

3. Data analysis

3.1. Statistics

We identified 225 CMEs fulfilling our selection criteria which we were able to associate with shocks at 1 AU. Of these 88 were associated with ESP events at 6.0 MeV. The number of ESP events diminished to 59 at 18.2 MeV. The 88 CME-driven shocks associated with the ESP events at proton energies 6.0 and 18.2 MeV are listed in Table A.2 in the Appendix.

Sixty-two (71%) out of the 88 events were associated with SEP events, and 74 (85%) with DH type II bursts at 6.0 MeV. At the higher energy SEP events and DH type II bursts were associated with 40 (68%) and 50 (84%) out of the 59 events, respectively. Both SEPs and DH type II radio bursts were associated with 59 (67%) ESP events at 6.0 MeV and with 39 (66%) events at 18.2 MeV.

3.2. Predicted shock transit speed

Shock transit speed (V_{TR}) represents the mean speed of transport of a shock in IP space when travelling from the Sun to 1 AU. In our previous study (Ameri et al., 2023) we found that the observed V_{TR} played a significant role in explaining the variation in the logarithm of the peak intensities of the ESP events ($\log_{10}[I_{ESP}^{peak}]$). The highest correlation coefficients of the $\log_{10}[I_{ESP}^{peak}]$ at different energies were found with the observed V_{TR} compared to other parameters related to CMEs at the Sun and IP shocks at 1 AU, but in order for the shock transit speed to be useful for ESP forecasting, it needs to be predicted from solar observations. In this work, we use the predicted shock transit speed as the primary parameter to forecast the peak intensities of ESP events.

Travel times of coronal mass ejections to 1 AU can be estimated using various methods (see, e.g., Gopalswamy et al., 2001; Vršnak et al., 2010; Corona-Romero et al., 2017, and references therein), and the results are naturally model-dependent. We estimate V_{TR} for our 88 events by using the method recently presented by Belov et al. (2022), which employs only CME data and solar X-ray flare location, which is assumed to be the launch site of the CME. Thus, an estimate of V_{TR} can be obtained well in advance of the shock arrival at 1 AU. The model of Belov et al. (2022) is based on a collection of 288 events for which the CME launch time and speed, solar longitude of the CME launch site, and the associated shock arrival time are reliably known. Using these events covering a wide range of CME speeds and solar longitudes and for which the transit speeds are known from the difference between the CME launch times and shock arrival times, one can estimate the transit speed of CMEs of interest as the weighted mean of similar events selected under certain conditions from the original database. For details of the method, see Belov et al. (2022). When calculating the transit speed, we used for the partial weight-factor, which depends on the CME speed, the form $s_v = |1 - (V_{Oi}/V_{CME})|$, where V_{Oi} are the CME speeds of the events in the database in the vicinity of the event under study.

Fig. 1 shows the scatter plot between the observed V_{TR} and the predicted V_{TR} of our events. It should be noted

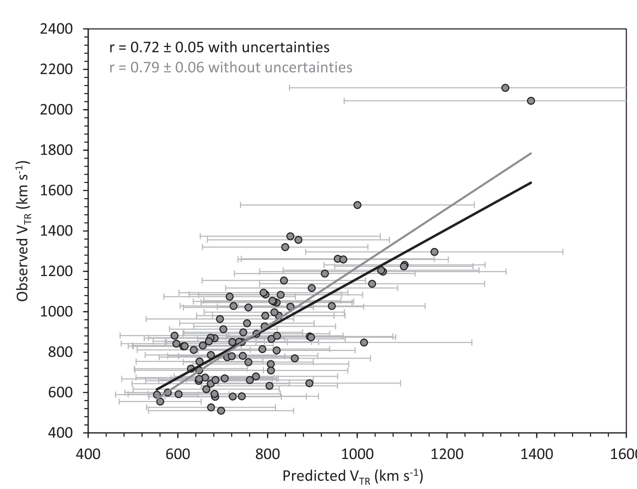

Fig. 1. Scatter plot of the observed shock transit speeds as function of the predicted shock transit speeds. The best-fit linear regression lines are shown by the black line for data points taking into account the uncertainties in the predicted transit speeds and the gray line for the case without the uncertainties. The calculated correlation coefficients with their standard deviations are shown in the figure.

that many of our events are the same as in the Belov et al. (2022) database. The correlation coefficient between the observed V_{TR} and the predicted V_{TR} is 0.79±0.06 without taking into account the uncertainties in the predicted transit speeds. The correlation coefficient is slightly smaller (0.72 ±0.05) when taking into account the uncertainties. The scatter plot and the correlation coefficient of our events are similar to those presented by Belov et al. (2022).

3.3. Correlation analysis

We investigated the dependence of the peak intensities of the ESP events at 1 AU on various parameters describing the characteristics of the CMEs and their associations observed at the Sun or in IP space. These parameters include the shock transit speed, the CME speed, the angular distance of the X-ray flare location from the disk centre (α), the soft X-ray flux, the peak intensity of the associated SEP event, and the duration of the DH type II radio burst. We carried out correlation studies of the ESP peak intensity for 1, 2, 3, and 4 explanatory variables to obtain the best correlations. The logarithmic scale was used for particle intensities, soft X-ray flux, and duration of DH type II burst in the calculation of correlation coefficients. We estimated the Pearson correlation coefficients and their uncertainties by using the bootstrapping method of sampling with replacement (for more details see Ameri et al., 2023).

The scatter plots of $\log_{10}[I_{ESP}^{peak}]$ as function of the predicted transit speed at energies 6.0 and 18.2 MeV are presented in Figs. 2 a and b, respectively. The error bars in Fig. 2 display the uncertainties in the calculated V_{TR}. We found strong correlation between $\log_{10}[I_{ESP}^{peak}]$ and the predicted V_{TR} as shown in Fig. 2. The correlation coefficients were 0.68 ± 0.05 at 6.0 MeV and 0.71 ± 0.06 at 18.2 MeV for the data points without taking into account the uncertainties in the calculated V_{TR}. Although the uncertainties are large for some events the correlation coefficients for the data with the uncertainties (0.66 ± 0.06 at 6.0 MeV and 0.69 ± 0.07 at 18.2 MeV) were similar to those without the uncertainties as shown in Figs. 2 a and b. For comparison we also calculated the correlation coefficients between $\log_{10}[I_{ESP}^{peak}]$ and the observed V_{TR} for the same events. They were 0.73 ± 0.04 at 6.0 MeV and 0.71 ± 0.05 at 18.2 MeV. This shows that the correlations of $\log_{10}[I_{ESP}^{peak}]$ with the predicted and observed V_{TR} are equal within uncertainties. It should be noted, however, that many ESP events in our current sample are associated with the same solar events as those in the Belov et al. (2022) database for predicting V_{TR}.

The dependence of $\log_{10}[\mathrm{I}_{\mathrm{ESP}}^{\mathrm{peak}}]$ on the CME parameters was also investigated. The CME linear speed ($V_{\mathrm{CME}}^{\mathrm{linear}}$) and the space speed ($V_{\mathrm{CME}}^{\mathrm{space}}$), and the angular distance from the disk centre were used as the CME parameters. We used the space speeds for the halo CMEs as given in the CDAW halo CME catalog (Gopalswamy et al., 2010). For 12 partial-halo CMEs we used the cone model presented by Xie et al. (2004) and the formula given by Gopalswamy et al. (2010) to calculate the CME space speed. The correlation coefficients of $\log_{10}[I_{ESP}^{peak}]$ *vs.* $V_{\mathrm{CME}}^{\mathrm{linear}}$ and $\log_{10}[\mathrm{I}_{\mathrm{ESP}}^{\mathrm{peak}}]$ *vs.* $V_{\mathrm{CME}}^{\mathrm{space}}$ were 0.55 ± 0.07 and 0.59 ± 0.05 at 6.0 MeV and 0.64 ± 0.07 and 0.68 ± 0.07 at 18.2 MeV, respectively, as presented in Table 1. At both energies the correlation of $\log_{10}[\mathrm{I}_{\mathrm{ESP}}^{\mathrm{peak}}]$ with $V_{\mathrm{CME}}^{\mathrm{space}}$ was stronger than with $V_{\mathrm{CME}}^{\mathrm{linear}}$. We found insignificant very weak correlations between $\log_{10}[\mathrm{I}_{\mathrm{ESP}}^{\mathrm{peak}}]$ and α(-0.23 ±0.09 at 6.0 MeV and -0.09 ±0.09 at 18.2 MeV). We also found a weak to moderate correlation between $\log_{10}[\mathrm{I}_{\mathrm{ESP}}^{\mathrm{peak}}]$ and the logarithm of soft X-ray flux ($\log_{10}$ [SXRF]) for solar flares related to the CMEs with the correlation coefficients of 0.32 ± 0.10 and 0.48 ± 0.09

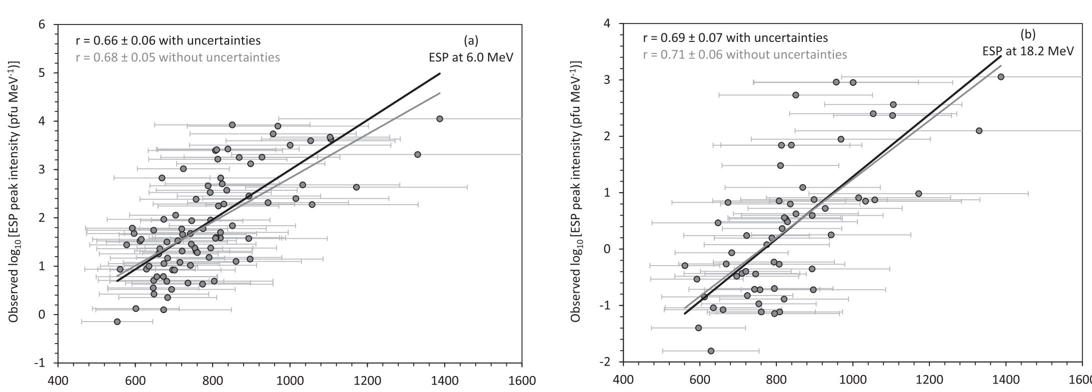

Fig. 2. Scatter plots of the observed logarithm of the ESP peak intensities as function of predicted shock transit speeds. The best-fit linear regression lines are shown by the black lines for data points taking into account the uncertainties in the predicted transit speeds and the gray lines for the case without the uncertainties. The calculated correlation coefficients with their standard deviations are shown in the panels.

Table 1
Correlation coefficients between the observed and calculated peak intensities of ESP events at 6.0 and 18.2 MeV using various parameters or combinations of parameters. For briefness, the letter symbols from A to F defined on the first row are used for the parameters in more than one-variable combinations. The p-value of the null-hypothesis that there is no correlation between the variables is given under each coefficient.

One explanatory variable:

Energy	V_{TR}[A]	V_{CME}^{linear}[B]	V_{CME}^{space}[C]	$\log_{10}$[SXRF] [D]	$\log_{10}[I_{SEP}^{peak}]$ [E]	$\log_{10}[D_{TII}]$ [F]
6.0 MeV	0.68 ± 0.05	0.55 ± 0.07	0.59 ± 0.05	0.32 ± 0.10	0.55 ± 0.08	0.43 ± 0.08
p-value	6.8×10^{-14}	3.9×10^{-8}	1.6×10^{-9}	3.2×10^{-3}	4.7×10^{-6}	1.1×10^{-4}
18.2 MeV	0.71 ± 0.06	0.64 ± 0.07	0.68 ± 0.07	0.48 ± 0.09	0.70 ± 0.08	0.32 ± 0.13
p-value	2.5×10^{-10}	4.5×10^{-8}	3.4×10^{-9}	1.1×10^{-4}	3.0×10^{-7}	0.01

Two explanatory variables:

Energy	AC	AD	AE	AF	CE	CD
6.0 MeV	0.70 ± 0.05	0.70 ± 0.05	0.75 ± 0.05	0.72 ± 0.05	0.65 ± 0.06	0.60 ± 0.06
p-value	7.7×10^{-13}	6.8×10^{-13}	1.9×10^{-11}	5.2×10^{-12}	1.4×10^{-7}	1.3×10^{-8}
18.2 MeV	0.73 ± 0.06	0.72 ± 0.05	0.80 ± 0.05	0.70 ± 0.07	0.74 ± 0.07	0.69 ± 0.07
p-value	1.6×10^{-9}	4.1×10^{-9}	1.8×10^{-8}	6.4×10^{-7}	1.8×10^{-6}	5.8×10^{-8}
Energy	CF	DE	DF	EF		
6.0 MeV	0.64 ± 0.06	0.58 ± 0.08	0.47 ± 0.08	0.62 ± 0.08		
p-value	1.7×10^{-8}	1.1×10^{-5}	1.8×10^{-4}	1.3×10^{-6}		
18.2 MeV	0.67 ± 0.07	0.73 ± 0.07	0.55 ± 0.09	0.74 ± 0.07		
p-value	4.0×10^{-6}	9.6×10^{-7}	3.8×10^{-4}	1.5×10^{-6}		

Three explanatory variables:

Energy	ACD	ACE	AEF	CEF	ADE	CDE
6.0 MeV	0.71 ± 0.05	0.76 ± 0.05	0.79 ± 0.04	0.70 ± 0.06	0.76 ± 0.05	0.66 ± 0.06
p-value	4.5×10^{-12}	9.6×10^{-11}	2.4×10^{-11}	8.9×10^{-8}	1.1×10^{-10}	7.6×10^{-7}
18.2 MeV	0.74 ± 0.06	0.82 ± 0.05	0.83 ± 0.05	0.79 ± 0.05	0.81 ± 0.05	0.76 ± 0.06
p-value	3.8×10^{-9}	1.5×10^{-8}	8.3×10^{-9}	4.2×10^{-7}	2.1×10^{-8}	1.8×10^{-6}

Four explanatory variables:

Energy	ACDE	ACEF	ADEF
6.0 MeV	0.77 ± 0.04	0.80 ± 0.04	0.80 ± 0.04
p-value	4.8×10^{-10}	9.4×10^{-11}	1.3×10^{-10}
18.2 MeV	0.83 ± 0.05	0.84 ± 0.05	0.84 ± 0.05
p-value	7.4×10^{-8}	5.8×10^{-8}	6.0×10^{-8}

at 6.0 and 18.2 MeV, respectively. Figs. 3 a and b show the scatter plots of $\log_{10}[I_{ESP}^{peak}]$ as function of $V_{CME}^{space}$and $\log_{10}$ [SXRF] at 18.2 MeV.

In the investigation of the dependence of $\log_{10}[I_{ESP}^{peak}]$ on the logarithm of the peak intensity of the SEP events ($\log_{10}[I_{SEP}^{peak}]$), we found a moderate correlation (0.55 ± 0.08) at 6.0 MeV while there was significantly higher correlation (0.70 ± 0.08) at 18.2 MeV as shown in Fig. 3c. We also investigated the dependence of $\log_{10}[I_{ESP}^{peak}]$ on the characteristics of DH type II radio bursts. The end-frequencies and durations of DH type II bursts can be used as parameters to describe the strength of shocks in IP space. We found a moderate correlation at 6.0 MeV and weak correlation at 18.2 MeV between $\log_{10}[I_{ESP}^{peak}]$ and the logarithm of the duration of DH type II radio burst ($\log_{10}[D_{TII}]$). The correlation coefficients were 0.43 ± 0.08 and 0.32 ± 0.13, respectively (See Table 1). Fig. 3d shows that the highest ESP peak intensities >100 pfu MeV^{-1}($\log_{10}[I_{ESP}^{peak}] > 2$) were associated with long duration DH type II bursts. The correlation coefficients at 6.0 and 18.2 MeV demonstrate that the correlations are energy dependent. With the exception of $\log_{10}[D_{TII}]$ the correlation coefficients increase with energy.

3.4. Correlations for combinations of parameters

In addition to the single explanatory variable correlations we also investigated correlations between the peak intensities of ESP events and various combinations of two or more explanatory variables. The most significant correlations between $\log_{10}[I_{ESP}^{peak}]$ and various single parameters or combinations of parameters are summarised in Table 1. It should be noted that the duration of DH type II bursts for some events was so long that their end times exceeded the ESP peak time. In such cases forecasting ESP peak intensities by using $\log_{10}[D_{TII}]$ would not be possible. For forecasting purposes we determined the upper limit of the end time of the DH type II bursts to be 24 h from the start time. This means that if the duration exceeds 24 h, then 24 h is used for forecasting $\log_{10}[I_{ESP}^{peak}]$. We selected the upper limit of 24 h based on that the strongest CMEs need at least 24 h to reach 1 AU. When we applied this upper limit for $\log_{10}[D_{TII}]$ we obtained similar correlation coefficients (0.43 ± 0.08 at 6.0 MeV and 0.30 ± 0.11 at 18.2 MeV) for $\log_{10}[I_{ESP}^{peak}]$ *vs.* $\log_{10}[D_{TII}]$ as when using the real durations. In general the predicted V_{TR}without uncertainties, $\log_{10}[D_{TII}]$ with the upper limit of 24 h, and

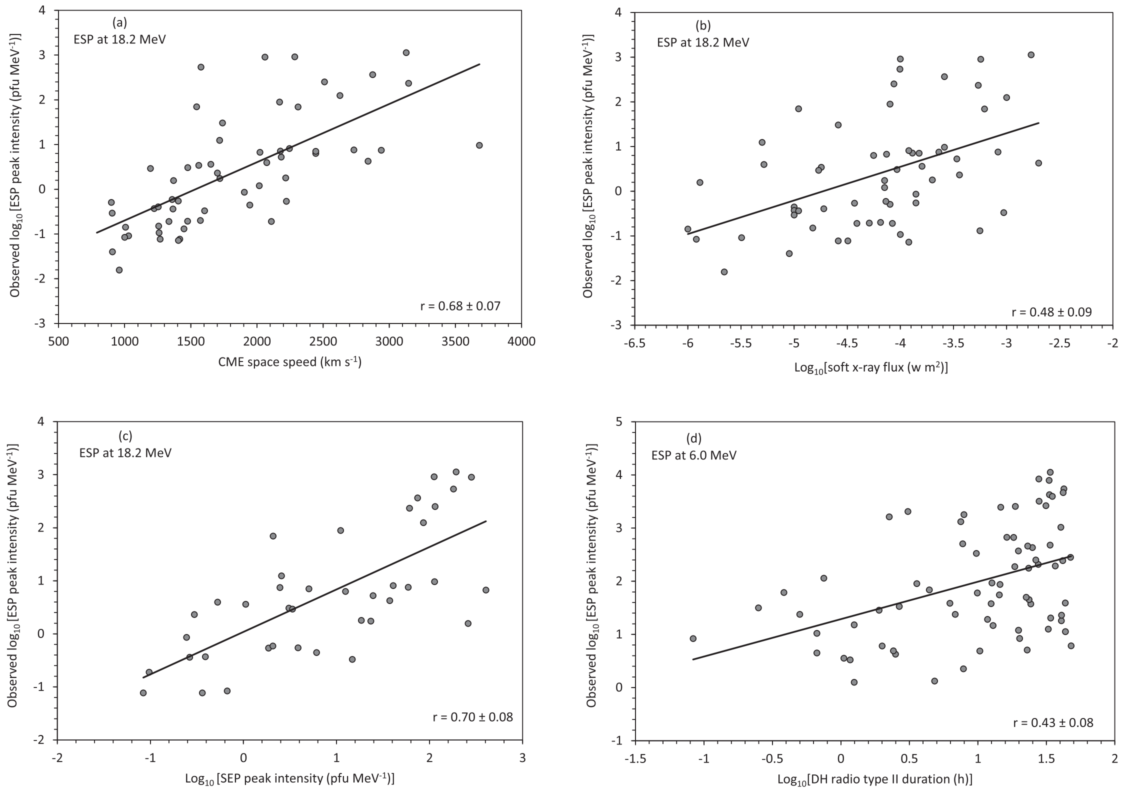

Fig. 3. Scatter plots of the observed logarithm of ESP peak intensities as function of the CME space speeds (a), the logarithm of soft X-ray fluxes (b), the logarithm of SEP peak intensities (c), and the logarithm of durations of DH type II bursts (d).

V_{CME}^{space} were used in all multiple linear regressions. The correlation coefficients presented in Table 1 are those between the logarithms of the observed ESP peak intensities and those calculated from the multiple linear regression equations.

For two explanatory variable combinations at the two energy ranges we found significant improvement in the correlation coefficients when using V_{TR} and $\log_{10}$ [I_{SEP}^{peak}] while there were slight improvement when using V_{TR} with V_{CME}^{space}, $\log_{10}$ [SXRF], or $\log_{10}$ [D_{TII}] (see Table 1). It is clear that the best two-variable combination explaining the peak intensity of an ESP event is V_{TR} combined with $\log_{10}$ [I_{SEP}^{peak}] with the correlation coefficients 0.75 ± 0.05 at 6.0 MeV and 0.80 ± 0.05 at 18.2 MeV. An SEP event is not associated with all ESP events. However, the number of ESP events without an SEP event is relatively small (∼29%) and the average ESP peak intensity without an SEP event is significantly lower than with an SEP event (see, e.g., Ameri et al., 2023). Adding a third and fourth parameter to the two variable combination slightly improves the correlation coefficients. The best three variable combinations were found to be V_{TR}, $\log_{10}$ [I_{SEP}^{peak}], and V_{CME}^{space}; V_{TR}, $\log_{10}$ [I_{SEP}^{peak}], and $\log_{10}$ [D_{TII}]; and V_{TR}, $\log_{10}$ [I_{SEP}^{peak}], and $\log_{10}$ [SXRF]. The highest correlation coefficients with three explanatory variables were found with the second combination (0.79 ± 0.04 at 6.0 MeV and 0.83 ± 0.05 at 18.2 MeV) as presented in Table 1. On the other hand the best three variable combination which only depends on electromagnetic observations of the Sun are V_{TR}, V_{CME}^{space}, and $\log_{10}$ [SXRF]. The correlation coefficients of this combination were 0.71 ± 0.05 at 6.0 MeV and 0.74 ± 0.06 at 18.2 MeV as shown in Fig. 4. Fig. 4 shows the logarithm of the observed ESP peak intensities as function of the logarithm of the ESP peak intensities calculated from these three variables. The calculated values are based on the multiple linear regression equation shown in each plot.

Finally certain combinations of four explanatory variables also slightly improve the correlation coefficients compared to the three variables combinations. The highest correlation coefficients were found for V_{TR}, $\log_{10}$ [I_{SEP}^{peak}], V_{CME}^{space}, and $\log_{10}$ [SXRF] (0.77 ± 0.04 at 6.0 MeV and 0.83 ± 0.05 at 18.2 MeV) and V_{TR}, $\log_{10}$ [I_{SEP}^{peak}], V_{CME}^{space}(or $\log_{10}$ [SXRF]), and $\log_{10}$ [D_{TII}] (0.80 ± 0.04 at 6.0 MeV and 0.84 ± 0.05 at 18.2 MeV) as shown in Table 1 and Fig. 5. Fig. 5 shows observed $\log_{10}$ [I_{ESP}^{peak}] as function of $\log_{10}$ [I_{ESP}^{peak}] calculated from these four variables. The calculated values are based on the multiple linear regression equation shown in each plot.

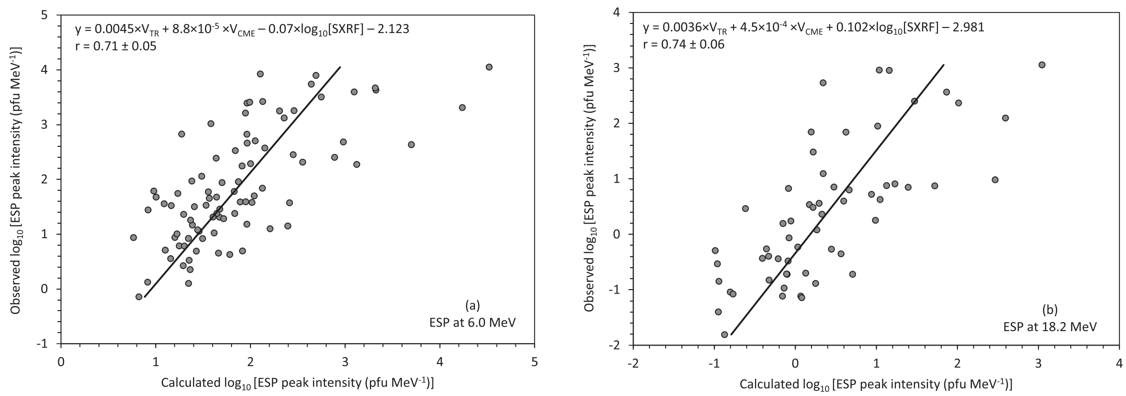

Fig. 4. (a) Scatter plot of the logarithm of the observed peak intensities of the ESP events as function of those calculated based on three explanatory variable (V_{TR}, V^{space}_{CME}, and $\log_{10}$ [SXRF]) regression at 6.0 MeV. (b) as (a), but at 18.2 MeV. The regression equation, the calculated correlation coefficient and its standard deviation are shown at the top of the panels. The black line is a linear fit line to the data points.

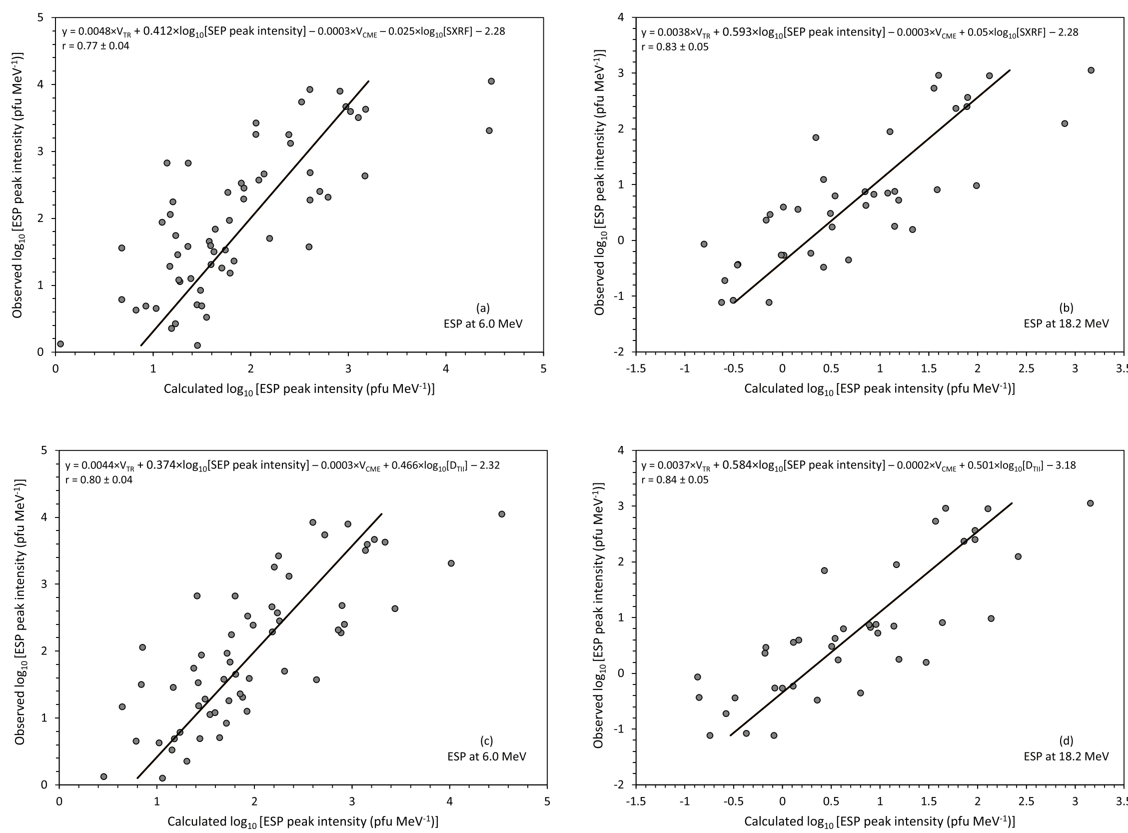

Fig. 5. (a) Scatter plot of the logarithm of the observed peak intensities of the ESP events as function of those calculated based on four explanatory variable (V_{TR}, $\log_{10}$ [I^{peak}_{SEP}], V^{space}_{CME}, and $\log_{10}$ [SXRF]) regression at 6.0 MeV. (b) as (a), but at 18.2 MeV. (c) as (a), but for V_{TR}, $\log_{10}$ [I^{peak}_{SEP}], V^{space}_{CME}, and $\log_{10}$ [D_{TII}]. (d) as (c), but at 18.2 MeV. The regression equation, the calculated correlation coefficient and its standard deviation are shown at the top of the panels. The black line is a linear fit line to data points.

3.5. Wait and lead times for forecasting

For long lead time forecasting using only coronagraph and X-ray observations (V_{TR}, V^{space}_{CME}, and $\log_{10}$ [SXRF]), the time required for measuring the CME speed determines the wait time before forecasting is possible. Consequently, the wait time can be defined as the time from the first to the last observation of the CME. The wait times for our 88 events range from 0.5 h to 7.9 h with the average and standard deviation of 3.1 ±1.5 h. At 6.0 MeV, the lead times,

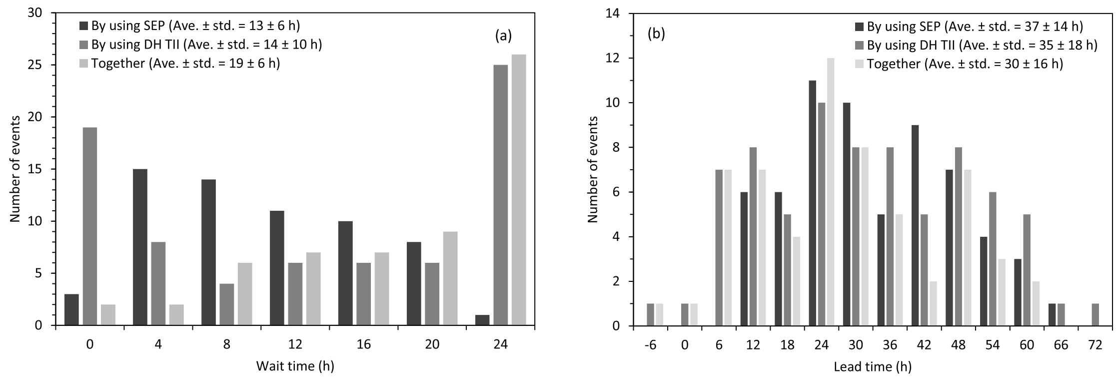

Fig. 6. (a) Distributions of the wait time and (b) the lead time for forecasting the peak intensity of ESP events by using the peak intensity of SEP events (black columns), the duration of DH type II bursts (dark gray), and both together (light gray) at 6.0 MeV. The averages and the standard deviations of the distributions are given in the panels.

from the time when the CME speed has been determined to the ESP peak time, range from 17.6 h to 77.7 h with the average and standard deviation of 47 ±13 h. At 18.2 MeV the wait and lead times are similar.

For medium lead time forecasting, when using also SEP or DH type II radio burst observations, the wait time is defined as the time from the CME lift-off to the observation time of the SEP peak intensity or the end of the DH type II burst. The lead time is then the time from the observation of the SEP peak intensity or the end of the DH type II burst to the ESP peak time. Therefore the combinations of multiple variables including $\log_{10}$ [I_{SEP}^{peak}] or/and $\log_{10}$ [D_{TII}] can be used for medium-lead time forecasting. We present the distributions of the wait and lead times for these cases at 6.0 MeV in Figs. 6 a and b. The bin widths in Figs. 6 a and b are 4 h and 6 h, respectively. The distributions of wait and lead times at 18.2 MeV are similar to Figs. 6 a and b. For the duration of DH type II bursts we used the upper limit at 24 h as explained in Section 3.4. The wait times range from 2.5 h to 27 h for $\log_{10}$ [I_{SEP}^{peak}] and from 0.38 h to 24 h for $\log_{10}$ [D_{TII}] with the average and standard deviation 13 ±6 h and 14 ±10 h, respectively. Roughly half of the events (52% out of 62 and 43% out of 74, respectively) had the wait time <12 h as shown in Fig. 6 a. When using $\log_{10}$ [I_{SEP}^{peak}] and $\log_{10}$ [D_{TII}] together the wait times are in the range 2.5 – 27 h with average and standard deviation of 19 ±6 h.

The lead times range from 12.4 h to 68.7 h with average and standard deviation of 37 ±14 h by using $\log_{10}$ [I_{SEP}^{peak}] and from −4.9h to 77.6 h with average and standard deviation of 35 ±18 h by using $\log_{10}$ [D_{TII}]. When using both parameters together the lead times are in the range −4.9–62.2 h with average and standard deviation of 30 ±16 h. When using $\log_{10}$ [I_{SEP}^{peak}] for forecasting, all events had lead times >12 h and 81% of the events had lead times >24 h as shown in Fig. 6. When forecasting using $\log_{10}$ [D_{TII}] or DH type II with $\log_{10}$ [I_{SEP}^{peak}] together and applying the upper limit of the duration of DH type II bursts of 24 h from the start time there was one event with negative lead time because the associated DH type II burst ends about 4.9 h after the ESP peak time. This event was the very energetic CME on 28th of October 2003 at 11:30 UT. Eight events (11%) had a lead time less than 12 h because the DH type II bursts end close to the ESP peak time. In general the distributions of lead times are broad with a maximum at 24 h and most of the events have lead times >12 h as shown in Fig. 6 b.

4. Summary and discussion

We have investigated the relations between the peak intensities of ESP events at 1 AU and parameters related to the solar sources and their associations observed at the Sun or in IP space. In addition to the primary parameter of the predicted shock transit speed, we used several other parameters, such as the CME speed and angular distance from the solar disk centre, soft X-ray flux, peak intensity of the SEP events, and duration of the DH type II radio bursts to study their relations with the peak intensities of ESP events. The purpose of this study is using these relations to suggest models for forecasting the ESP peak intensities.

We searched for the associations between full and partial halo CMEs with CME linear speeds >400 kms^{-1}-launched from the front side of the solar disk and IP shocks at 1 AU. Then we investigated energetic particle observations provided by SEPEM server at two energy ranges, 5.0–7.2 MeV (nominal energy 6.0 MeV) and 15.1–21.9 MeV (18.2 MeV), in order to identify particle enhancements at the time of these shock passages at 1 AU. We found 88 CME-driven IP shocks associated with ESP events at 6.0 MeV during the time period 1996 – 2015. At the higher energy of 18.2 MeV the number of events decreased to 59.

We calculated the predicted shock transit speeds (V_{TR}) and their uncertainties for our events based on the model of ICME transit speeds by Belov et al. (2022). As noted in Section 3.2, the estimated arrival times are model-dependent, and thus correlations with observed values can also vary. Using the model of Belov et al. (2022) the correlation coefficients between the observed and calculated V_{TR}were 0.79± 0.06 without taking into account the uncertainties and 0.72± 0.05 when the uncertainties were included. Our results are similar with the findings (0.80 ± 0.04) by Belov et al. (2022) for the events in their database. It should be noted, however, that many ESP events in our current sample are associated with the same solar events as those in the Belov et al. (2022) database for predicting V_{TR}. This can to some extent explain the high correlation between $V_{TR}$and $\log_{10}$ [I_{ESP}^{peak}], and the full validation of our model on the part of $V_{TR}$is still pending on using an independent set of ESP events.

We investigated which parameters characterising CMEs and their associations best explained the observed $\log_{10}$ [I_{ESP}^{peak}] at 6.0 and 18.2 MeV. The highest correlation coefficient with a single explanatory variable was found between $\log_{10}$ [I_{ESP}^{peak}] and the predicted V_{TR}. The correlation coefficients were 0.68 ±0.05 at 6.0 MeV and 0.71 ±0.06 at 18.2 MeV for the data points without taking into account the uncertainties in the calculated V_{TR}. When using the uncertainties the correlation was slightly worse (see Fig. 2). The high correlation between $V_{TR}$and $\log_{10}$ [I_{ESP}^{peak}] indicates that the transport conditions from the Sun to 1 AU significantly affect the strength of IP shocks driven by CMEs and their ability to accelerate particles at 1 AU.

In comparison, the correlation coefficients between $\log_{10}$ [I_{ESP}^{peak}] and CME speeds were 0.55 ± 0.07 and 0.64 ± 0.07 for CME linear speed and 0.59 ± 0.05 and 0.68 ± 0.07 for CME space speed at 6.0 and 18.2 MeV, respectively. Thus, the correlation was slightly better when using the space speed instead of the linear speed. Mäkelä et al. (2011) found that the correlation coefficient between $\log_{10}$ [I_{ESP}^{peak}] and CME linear speeds is 0.69. We found only a very weak correlation between $\log_{10}$ [I_{ESP}^{peak}] and the angular distance of the CME launch site from the disk centre (−0.23 ±0.09 at 6.0 MeV and −0.09 ±0.09 at 18.2 MeV). There was also a weak to moderate correlation between $\log_{10}$ [I_{ESP}^{peak}] and $\log_{10}$ [SXRF]. The correlation coefficients were 0.32 ± 0.10 at 6.0 MeV and 0.48 ± 0.09 at 18.2 MeV (see Table 1).

We investigated the correlations of $\log_{10}$ [I_{ESP}^{peak}] with $\log_{10}$ [I_{SEP}^{peak}] observed when the shock was near the Sun and $\log_{10}$ [D_{TII}] observed in IP space. We found a significant correlation between ESP peak intensities and the associated SEP peak intensities (0.55 ±0.08) at 6.0 MeV, and the correlation coefficient still increased with energy being 0.70 ±0.08 at 18.2 MeV. This indicates that if the shock is able to accelerate particles near the Sun, it is often capable to accelerate particles also at 1 AU. The exact level of the ESP peak intensities compared to the SEP peak intensities varies depending on the effects of the transport conditions from the Sun to 1 AU and on the strength of the shocks driven by the CMEs (*i.e.* V_{TR}). This result agrees with the findings by Luhmann and Mann (2007) and Ameri et al. (2023). For CME-driven shocks related to DH type II radio bursts we found a moderate to weak correlation between $\log_{10}$ [I_{ESP}^{peak}] and $\log_{10}$ [D_{TII}] with correlation coefficients of 0.43 ±0.08 at 6.0 MeV and 0.32 ±0.13 at 18.2 MeV. The relatively good correlation between $\log_{10}$ [I_{ESP}^{peak}] and $\log_{10}$ [D_{TII}] in particular at 6.0 MeV as shown in Fig. 3 d implies that the characteristics of DH type II bursts are related to the strength of IP shocks, and their duration can be used as a parameter to describe the ESP peak intensity in many cases.

The correlations of $\log_{10}$ [I_{ESP}^{peak}] for various combinations of two or more explanatory variables were investigated. For two explanatory variables, combining $V_{TR}$with other solar parameters led to improvements in the correlation coefficients as presented in Table 1. The best two-variable combination giving the largest improvement in explaining the peak intensities of ESP events was V_{TR}combined with $\log_{10}$ [I_{SEP}^{peak}] at the two energies. The correlation coefficients between the calculated $\log_{10}$ [I_{ESP}^{peak}] from these two parameters and the observed $\log_{10}$ [I_{ESP}^{peak}] were 0.75 ±0.05 at 6.0 MeV and 0.80 ±0.05 at 18.2 MeV. These results demonstrate that for SEP – ESP events the $\log_{10}$ [I_{ESP}^{peak}] can be best estimated using $V_{TR}$and $\log_{10}$ [I_{SEP}^{peak}]. Adding one or two of the three parameters V_{CME}^{space}, $\log_{10}$ [SXRF], or $\log_{10}$ [D_{TII}] to the combination of $V_{TR}$and $\log_{10}$ [I_{SEP}^{peak}] slightly improves the correlation coefficients as presented in Table 1. Stepwise regression using every relevant variable reveals that $V_{TR}$and $\log_{10}$ [I_{SEP}^{peak}] are the strongest explanatory variables for $\log_{10}$ [I_{ESP}^{peak}]. When using a four explanatory variable combination, the highest correlation coefficients of observed and calculated $\log_{10}$ [I_{ESP}^{peak}] were 0.77 ± 0.04 at 6.0 MeV and 0.83 ± 0.05 at 18.2 MeV when the calculated $\log_{10}$ [I_{ESP}^{peak}] was derived from V_{TR}, $\log_{10}$ [I_{SEP}^{peak}], V_{CME}^{space}, and $\log_{10}$ [SXRF] and 0.80 ± 0.04 at 6.0 MeV and 0.84 ± 0.05 at 18.2 MeV when using V_{TR}, $\log_{10}$ [I_{SEP}^{peak}], V_{CME}^{space}(or $\log_{10}$ [SXRF]), and $\log_{10}$ [D_{TII}] (Table 1 and Fig. 5).

Although there are strong correlations between the ESP peak intensities and combinations of three or four explanatory variables, and our models can therefore be used for forecasting the peak intensities, their predictive power for the occurrence of ESP events is weak. Only 88 ESP events at 6.0 MeV were observed for 225 CMEs associated with shocks at 1 AU. The predictive power might, however, be improved when using higher thresholds for the CME space speeds or predicted shock transit speeds.

In case of applying only solar observations obtained close to the CME lift-off time the best relation for forecasting of $\log_{10}$ [I_{ESP}^{peak}] is the three explanatory variable combination including V_{TR}, V_{CME}^{space}, and $\log_{10}$ [SXRF] with correlation coefficient 0.71 ± 0.05 at 6.0 MeV and 0.74 ± 0.06 at 18.2 MeV (Fig. 4). In this case the average wait and lead times with their standard deviations are typically 3.1 ± 1.5 h and 47 ± 13 h, respectively. If the combination includes $\log_{10}$ [I_{SEP}^{peak}] or $\log_{10}$ [D_{TII}], which are measured when the shock is near the Sun or in IP space, the forecasting of $\log_{10}$ [I_{ESP}^{peak}] has longer wait and shorter lead times. For all events at 6.0 MeV the average and standard deviation of the wait times were 13 ± 6 h for $\log_{10}$ [I_{SEP}^{peak}] and 14 ± 10 h for $\log_{10}$ [D_{TII}], while the lead times were 37 ± 14 h for $\log_{10}$ [I_{SEP}^{peak}] and 35 ± 18 h for $\log_{10}$ [D_{TII}]. When using $\log_{10}$ [I_{SEP}^{peak}] and $\log_{10}$ [D_{TII}] together the wait and lead times were 19 ± 6 h and 30 ± 16 h (Fig. 6).

5. Conclusions

We investigated the correlations between ESP peak intensities and various parameters characterising the coronal mass ejections and their associations. We found the strongest correlation with the predicted shock transit speeds (0.68 ± 0.05 at 6.0 MeV and 0.71 ± 0.06 at 18.2 MeV). Moderate to strong correlations were found with the CME space speeds and the SEP peak intensities and weak to moderate correlations with the soft X-ray fluxes and the duration of DH type II radio bursts. The correlations were energy dependent.

Based on the combinations of three and four explanatory variables we suggest two empirical methods, which can be used for long lead time and medium lead time forecasting of the ESP peak intensities. For long lead time forecasting the three parameters used as input for calculating the logarithm of the ESP peak intensities are the shock transit speed, CME space speed, and logarithm of the soft X-ray flux. These three parameters can be measured or calculated soon after the CME lift-off time. The correlation coefficients between the observed and calculated logarithm of ESP peak intensities were 0.71 ± 0.05 at 6.0 MeV and 0.74 ± 0.06 at 18.2 MeV. Adding the logarithm of the SEP peak intensity and the logarithm of the duration of DH type II radio bursts together with the shock transit speed and CME space speed (or logarithm of the soft X-ray flux) significantly improves the correlation coefficients. These four explanatory variable combinations can be used as input for calculating ESP peak intensities for medium lead time forecasting. SEP peak intensities and the duration of DH type II radio bursts are measured when the shock is close to the Sun or in IP space. The highest correlation coefficients were 0.80 ± 0.04 at 6.0 MeV and 0.84 ± 0.05 at 18.2 MeV. This medium lead time forecasting provides an average warning time, i.e. the time from the observation of the SEP peak intensity and DH type II burst till the ESP peak time, of 30 ±16 h. For long lead time forecasting using only coronagraph and X-ray observation, the average warning time is 47 ±13 h.

Declaration of competing interest

The authors declare that they have no known competing financial interests or personal relationships that could have appeared to influence the work reported in this paper.

Acknowledgements

The authors gratefully acknowledge the various online data centers of NOAA and NASA. The LASCO CME catalog is generated and maintained by the Center for Solar Physics and Space Weather, The Catholic University of America in cooperation with the Naval Research Laboratory and NASA. Part of the data analysis for this article was generated using the Real Statistics Resource Pack software maintained by Charles Zaiontz. R.V. acknowledges funding from the European Union's Horizon 2020 research and innovation programme under grant agreement No 101004159 (SERPENTINE) and funding from the Research Council of Finland (project 336809, FORESAIL).

Appendix A. Table A.2

Table A.2
List of CME-driven IP shocks with an ESP event at proton energies 6.0 and 18.2 MeV with associated solar flares, DH type II radio bursts, and SEP events during 1996–2015.

N:o	CME		Solar flare		DH TII	IP shock			SEP peak intensity		ESP peak intensity	
	Date and Time [a] dd/mm hh:mm	Space speed[b] km s^{-1}	Class	Location	Duration[c] h	Date and Time[d] dd/mm hh:mm	Observed V_{TR} km s^{-1}	Predicted V_{TR} km s^{-1}	6.0 MeV pfu MeV^{-1}	18.2 MeV pfu MeV^{-1}	6.0 MeV pfu MeV^{-1}	18.2 MeV pfu MeV^{-1}
	1997											
1	06/11 12:10	1604	X9.4	S18W63	20.17	09/11 10:03 W	510	696 ±162	111	14.8	8.38	0.33
	1998											
2	20/04 10:07	2160*	M1.4	S43W90	43.58	23/04 17:29 W	527	674 ±144	133	—	11.3	—
3	27/04 08:56	1482	X1.0	S16E50	0.67	30/04 08:43 W	581	742 ±171	—	—	10.5	—
4	05/11 20:44	1335	M8.4	N22W18	34.00	08/11 04:41 W	751	757 ±145	34.2	0.097	20.4	0.19
	2000											
5	10/02 02:30	1108	C7.3	N31E04	0.08	11/02 23:34 W	914	701 ±120	—	—	8.33	—
6	04/04 16:32	1217	C9.7	N16W66	0.25	06/04 16:32 W	869	682 ±157	92.4	—	31.7	—
7	06/06 15:54	1348	X2.3	N20E18	41.67	08/06 08:41A	1021	757 ±145	67.6	—	244	—
8	11/07 13:27	1260	X1.0	N18E27	0.50	13/07 09:43 W	943	754 ±150	—	—	23.8	0.107
9	14/07 10:54	2061	X5.7	N22W07	28.00	15/07 14:15A	1529	1000 ±261	422	282	3200	900
10	25/07 03:30	900	M8.0	N06W08	—	28/07 06:38 W	555	561 ±91	—	—	8.64	0.51
11	09/08 16:30	1007	C1.0	N20W11	—	11/08 18:49 W	829	612 ±112	—	—	33.2	0.142
12	12/08 14:54	1110*	C3.2	N13W46	—	14/08 21:36A	754	648 ±141	31.9	—	2.66	—
13	12/09 11:54	1946	M1.0	S17W09	24.33	15/09 04:27 W	646	893 ±203	264	6.1	37.4	0.445
14	10/10 00:26	903	C6.7	N01W14	—	12/10 22:33 W	590	553 ±92	—	—	0.716	—
15	01/11 16:26	960	C2.2	S17E39	—	04/11 02:25 W	718	629 ±126	—	—	8.7	0.016
16	08/11 23:06	2023*	M7.4	N10W77	12.67	11/11 04:12 W	786	673 ±146	706	403	93.1	6.71
	2001											
17	20/01 21:30	1647	M7.7	S07E46	2.50	23/01 10:49 W	680	774 ±182	2.9	—	4.25	—
18	28/01 15:54	1140*	M1.5	S04W59	1.25	31/01 08:35 W	644	673 ±175	54.1	—	1.26	—
19	25/03 17:06	908	C9.0	N16E25	—	27/03 18:07 W	842	597 ±123	—	—	47.6	0.04
20	29/03 10:26	1130	X1.7	N20W19	19.80	31/03 01:14 W	1075	715 ±147	16.4	—	12	—
21	02/04 22:06	2840 *	X20	N17W78	4.42	04/04 14:41 W	1025	851 ±163	104	37.4	68.8	4.24
22	05/04 17:06	1476	M5.1	S24E50	—	07/04 17:56 W	850	743 ±171	—	—	47.5	0.193
23	06/04 19:30	1449	X5.6	S21E31	6.25	08/04 11:20 W	1046	820 ±168	—	—	38.7	0.13
24	10/04 05:30	2940	X2.3	S23W09	18.60	11/04 16:17 W	1199	1057 ±275	107	2.47	188	7.47
25	15/04 14:07	1450*	X14.	S20W85	22.92	18/04 00:49 W	710	647 ±144	176	—	5.1	—
26	26/04 12:30	1257	M1.5	N20W05	40.33	28/04 05:00 W	1029	724 ±119	—	—	1040	0.15
27	24/09 10:31	2875	X2.6	S16E23	33.25	25/09 20:17 W	1232	1106 ±180	321	74.5	4260	366
28	19/10 16:50	1051	X1.6	N15W29	47.92	21/10 16:40 W	871	673 ±138	3.84	—	6.1	—
29	22/10 15:06	1603	M6.7	S21E18	2.42	25/10 08:59 W	634	804 ±152	16.9	—	4.92	—
30	04/11 16:35	2286	X1.0	N06W18	42.50	06/11 01:25A	1262	956 ±215	143	112	5470	913
31	22/11 23:30	1577	M9.9	S17W36	27.83	24/11 05:51 W	1374	851 ±201	363	181	8410	538
32	26/12 05:30	1720*	M7.1	N08W54	23.67	29/12 05:17 W	581	722 ±164	99.3	23.4	45.2	1.74
	2002											
33	15/03 23:06	1297	M2.2	S08W03	0.75	18/03 13:14 W	670	704 ±120	16.2	—	114	—
34	18/03 02:54	1223	M1.0	S10W30	2.67	20/03 13:05A	775	710 ±151	88.8	0.39	33.7	0.37
35	17/04 08:26	1417	M2.6	S14W34	43.50	19/04 08:25 W	866	809 ±165	15.23	0.362	39.1	0.077
36	21/04 01:27	2396	X1.5	S14W84	22.50	23/04 05:00 W	809	820 ±175	505	—	50.1	—
37	22/05 03:50	1718	C5.0	S30W34	—	23/05 10:44 W	1356	869 ±203	130	2.57	1780	12.4
38	15/07 21:30	1560*	M1.8	N19W01	7.75	17/07 15:55 W	981	825 ±148	—	—	506	3.43
39	26/07 22:06	1071	M8.7	S19E26	1.05	29/07 12:40A	658	646 ±118	—	—	3.58	—
40	16/08 12:30	1937	M5.2	S14E20	32.67	18/08 18:40 W	769	860 ±169	7.5	—	12.6	—
41	05/09 16:54	2074	C5.2	N09E28	47.45	07/09 16:22 W	878	894 ±186	30.3	0.528	283	3.96
42	24/11 20:30	1212	C6.4	N20E35	0.67	26/11 21:10A	851	736 ±162	4.75	—	4.5	—

Table A.2 (*continued*)

N:o	CME Date and Time [a] dd/mm hh:mm	CME Space speed[b] km s^{-1}	Solar flare Class	Solar flare Location	DH TII Duration[c] h	IP shock Date and Time[d] dd/mm hh:mm	IP shock Observed V_{TR} km s^{-1}	Predicted V_{TR} km s^{-1}	SEP peak intensity 6.0 MeV pfu MeV^{-1}	SEP peak intensity 18.2 MeV pfu MeV^{-1}	ESP peak intensity 6.0 MeV pfu MeV^{-1}	ESP peak intensity 18.2 MeV pfu MeV^{-1}
	2003											
43	28/05 00:50	1701	X3.6	S07W20	23.50	29/05 18:38 W	998	815 ±156	6.64	0.297	176	2.31
44	29/05 01:27	1407	X1.2	S06W37	6.83	30/05 15:53 W	1086	795 ±170	—	—	23.8	0.072
45	28/10 11:30	3128	X17.0	S16E08	33.75	29/10 05:58A	2044	1387 ±416	488	193	11200	1130
46	29/10 20:54	2628	X10.0	S15W02	3.08	30/10 16:19A	2109	1330 ±481	518	86	2050	125
47	02/11 17:30	2733	X8.3	S14W56	7.50	04/11 06:46 W	1117	898 ±192	559	59	1320	7.57
48	18/11 08:50	2109	M3.9	N00E18	—	20/11 08:35 W	874	897 ±189	—	—	14.1	0.19
	2004											
49	07/01 04:06	1850*	M4.5	N02E76	2.00	09/01 09:25 W	779	656 ±157	—	—	6.07	—
50	20/01 00:06	1248	C5.5	S13W09	—	22/01 01:04A	850	721 ±123	—	—	20.6	—
51	11/04 04:30	1930 *	C9.6	S16W46	1.25	12/04 18:27 W	1095	791 ±188	82.1	—	15.2	—
52	25/07 14:54	1544	M1.1	N08W33	31.42	26/07 22:25 W	1320	839 ±185	53.1	2.09	2650	69.8
53	07/11 16:54	2218	X2.0	N09W17	27.58	09/11 09:25 W	1029	943 ±208	428	18.5	207	1.79
	2005											
54	15/01 23:07	3682	X2.6	N15W05	25.00	17/01 07:15A	1297	1172 ±287	362	113.3	431	9.62
55	19/01 08:30	2178	X1.3	N15W51	14.67	21/01 16:47A	741	807 ±174	—	—	2470	7.13
56	13/05 17:12	2171	M8.0	N12E11	33.17	15/05 02:10 W	1259	969 ±234	380	11.1	7930	89.1
57	14/07 10:54	2115	X1.6	N11W90	1.90	16/07 16:10 W	782	745 ±167	43.2	—	28.6	—
58	22/08 17:30	2445	M5.6	S13W65	19.75	24/08 05:35 W	1155	836 ±182	267	12.5	373	6.31
59	09/09 19:48	2311	X6.2	S12E67	2.25	11/09 01:00A	1051	813 ±179	—	—	1630	69.3
60	13/09 20:00	2445	X1.5	S09E10	33.67	15/09 08:36 W	1138	1033 ±251	73	5.05	481	7.06
	2006											
61	13/12 02:54	2184	X3.4	S06W23	7.92	14/12 13:51 W	1189	927 ±202	41.9	24.7	1800	5.27
62	14/12 22:30	1139	X1.5	S06W46	1.17	16/12 17:34 W	965	694 ±165	62.7	—	3.33	—
	2010											
63	01/08 13:42	1030	C3.2	N20E36	—	03/08 17:05 W	811	635 ±126	—	—	10.1	0.091
	2011											
64	15/02 02:24	960	X2.2	S20W10	4.83	18/02 00:49 W	592	601 ±112	1.23	—	1.33	—
65	07/03 20:00	2223	M3.7	N31W53	12.50	10/03 06:10A	709	807 ±172	24	1.86	38	0.54
66	04/08 04:12	1477	M9.3	N19W36	36.75	05/08 18:40 W	1084	829 ±183	42.3	3.08	194	3.05
67	22/09 10:48	1905	X1.4	N09E89	12.92	25/09 10:44 W	579	683 ±148	0.59	0.245	14.7	0.86
68	24/09 12:48	2018	M7.1	N10E56	9.92	09/26 11:44 W	891	775 ±164	—	—	60.3	1.2
69	26/11 07:12	1001	C1.2	N17W49	40.75	28/11 21:00 W	674	660 ±154	108	0.67	18.1	0.084
	2012											
70	19/01 14:36	1269	M3.2	N32E22	11.75	22/01 05:33 W	662	760 ±141	6.33	0.084	19.2	0.077
71	23/01 04:00	2511	M8.7	N28W21	35.00	24/01 14:40 W	1206	1053 ±219	236	115	3950	252
72	07/03 00:24	3146	X5.4	N17E27	42.00	08/03 10:30 W	1225	1104 ±154	260	61	4670	234
73	14/06 14:12	1254	M1.9	S17E06	—	16/06 19:34 W	780	720 ±119	—	—	59.1	0.403
74	12/07 16:48	1405	X1.4	N13W01	16.25	14/07 17:39 W	853	669 ±124	34.3	3.87	671	0.546
75	17/07 13:48	1195*	M1.7	S28W65	14.33	20/07 04:30A	668	647 ±173	41.6	3.37	55.4	2.92
76	28/09 00:12	1093	C3.7	N09W32	10.33	30/09 22:18 W	594	681 ±147	6.44	—	4.89	—
	2013											
77	15/03 07:12	1366	M1.1	N11E12	14.50	17/03 05:21 W	898	746 ±132	6.59	0.264	87.2	0.362
78	11/04 07:24	1369	M6.5	N09E12	7.83	13/04 22:13 W	662	684 ±127	28.5	—	2.26	—
79	22/05 13:26	1491	M5.0	S18W70?	40.83	24/05 17:26 W	616	663 ±163	430	—	23	—

(*continued on next page*)

Table A.2 (*continued*)

N:o	CME Date and Time [a] dd/mm hh:mm	CME Space speed[b] km s^{-1}	Solar flare Class	Solar flare Location	DH TII Duration[c] h	IP shock Date and Time[d] dd/mm hh:mm	IP shock Observed V_{TR} km s^{-1}	Predicted V_{TR} km s^{-1}	SEP peak intensity 6.0 MeV pfu MeV^{-1}	SEP peak intensity 18.2 MeV pfu MeV^{-1}	ESP peak intensity 6.0 MeV pfu MeV^{-1}	ESP peak intensity 18.2 MeV pfu MeV^{-1}
80	29/09 22:12	1370	C1.3	N17W29	23.12	02/10 01:16 W	815	788 ±150	107	260	460	1.57
	2014											
81	07/01 18:24	2246	X1.2	S15W11	26.45	09/01 19:31A	848	1015 ±241	101	40.8	252	8.13
82	17/02 05:12	790*	C6.6	S14W05	—	20/02 02:51A	600	577 ±95	—	—	27.7	—
83	18/04 13:26	1359	M7.3	S20W34	9.75	20/04 10:20 W	927	793 ±158	57	2.07	335	0.59
84	10/09 18:00	1652	X1.6	N14E02	18.25	12/09 17:17 W	881	821 ±147	9.1	1.06	668	3.61
85	21/12 12:12	906	M1.0	S14W25	0.38	23/12 11:30A	882	592 ±121	—	—	61.4	0.293
	2015											
86	15/03 01:48	932	C9.1	S22W25	—	17/03 04:00 W	830	615 ±126	6.67	—	36	—
87	21/60 02:36	1740	M2.6	N12E16	18.78	22/06 18:08 W	1055	810 ±153	—	—	2570	30.4
88	22/06 18:36	1573	M6.5	N12W08	3.58	24/06 13:07 W	980	795 ±153	—	—	90.4	0.2

[a] Date and time of the first appearance in LASCO C2.
[b] *indicates a partial-halo CME.
[c] The time period from the start time to the end time of DH type II radio burst.
[d] W and A refer to the Wind and Advanced Composition Explorer spacecraft in which the IP shocks were observed.

References

Ameri, D., Valtonen, E., Al-Sawad, A., Vainio, R., 2023. Relationships between energetic storm particle events and interplanetary shocks driven by full and partial halo coronal mass ejections. Adv. Space Res. 71, 2521–2533. https://doi.org/10.1016/j.asr.2022.12.014.

Belov, A., Shlyk, N., Abunina, M., Abunin, A., Papaioannou, A., 2022. Estimating the transit speed and time of arrival of interplanetary coronal mass ejections using CME and solar flare data. Universe 8, 327. https://doi.org/10.3390/universe8060327.

Berdichevsky, D., Szabo, A., Lepping, R., Viñas, A., Mariani, F., 2000. Interplanetary fast shocks and associated drivers observed through the 23rd solar minimum by Wind over its first 2.5 years. J. Geophys. Res. 105, 27289–27314. https://doi.org/10.1029/1999JA000367.

Brueckner, G.E., Howard, R.A., Koomen, M.J., et al., 1995. The Large Angle Spectroscopic Coronagraph (LASCO). Sol. Phys. 162, 357–402. https://doi.org/10.1007/BF00733434.

Bryant, D.A., Cline, T.L., Desai, U.D., McDonald, F.B., 1962. Explorer 12 observations of solar cosmic rays and energetic storm particles after the solar flare of September 28, 1961. J. Geophys. Res. 67, 4983–5000. https://doi.org/10.1029/JZ067i013p04983.

Cohen, C.M.S., 2006. Observations of energetic storm particles: An overview. Washington DC Am. Geophys. Union Geophys. Monograph Series 165, 275–282. https://doi.org/10.1029/165GM26.

Corona-Romero, P., Gonzalez-Esparza, J., A., Perez-Alanis, C.A., et al. 2017, Calculating travel times and arrival speeds of CMEs to Earth: An analytic tool for space weather forecasting, Space Weather, 15, 464–483. https://doi.org/10.1002/2016SW001489.

Crosby, N., Heynderickx, D., Jiggens, P., et al., 2015. SEPEM: a tool for statistical modelling the solar energetic particle environment. Space Weather 13, 406–426. https://doi.org/10.1002/2013SW001008.

Dierckxsens, M., Tziotziou, K., Dalla, S., et al., 2015. Relationship between solar energetic particles and properties of flares and CMEs: Statistical Analysis of Solar Cycle 23 Events. Sol. Phys. 290, 841–874. https://doi.org/10.1007/s11207-014-0641-4.

Giacalone, J., 2012. Energetic charged particles associated with strong interplanetary shocks. Astrophys. J. 761, 28. https://doi.org/10.1088/0004-637X/761/1/28.

Gopalswamy, N., Lara, A., Yashiro, S., Kaiser, M., Howard, R., 2001. Predicting the 1-AU arrival times of coronal mass ejections. J. Geophys. Res. 106, 29207–29218. https://doi.org/10.1029/2001JA000177.

Gopalswamy, N., Xie, H., Mäkelä, P., et al., 2010. Interplanetary shocks lacking type II radio bursts. Astrophys J 710, 1111–1126. https://doi.org/10.1088/0004-637X/710/2/1111.

Gopalswamy, N., Yashiro, S., Michalek, G., et al., 2010. A Catalog of Halo Coronal Mass Ejections from SOHO. Sun and Geosphere 5, 7–16, https://ui.adsabs.harvard.edu/abs/2010SunGe...5....7G.

Gopalswamy, N., Mäkelä, P., Yashiro, S., 2019. A Catalog of Type II radio bursts observed by Wind/WAVES and their Statistical Properties. Sun and Geosphere 14, 111–121, https://doi.org/10.31401/SunGeo.2019.02.03.

Ho, G.C., Lario, D., Decker, R.B., Smith, C.W., Hu, Q., 2008. Transient Shocks and Associated Energetic Particle Distributions Observed by ACE during Cycle 23. In: Li, G. et al. (Eds.), AIP Conference Proceeding 1039, pp. 184–189. https://doi.org/10.1063/1.2982443, New York.

Huttunen-Heikinmaa, K., Valtonen, E., 2009. Interplanetary fast forward shocks and energetic storm particle events above 1.5 MeV. Ann. Geophys. 27, 767–779. https://doi.org/10.5194/angeo-27-767-2009.

Jian, L., Russell, C.T., Luhmann, J.G., Skoug, R.M., 2006. Properties of Stream Interactions at One AU During 1995–2004. Sol. Phys. 239, 337–392. https://doi.org/10.1007/s11207-006-0132-3.

Kouloumvakos, A., Nindos, A., Valtonen, E., et al., 2015. Properties of solar energetic particle events inferred from their associated radio emission. Astron. Astrophys. 580, A80. https://doi.org/10.1051/0004-6361/201424397.

Lindsay, G.M., Russell, C.T., Luhmann, J.G., Gazis, P., 1994. On the sources of interplanetary shocks at 0.72 AU. J. Geophys. Res. 99, 11–18. https://doi.org/10.1029/93JA02666.

Luhmann, J.G., Mann, Adam, 2007. Relative fluxes of shock and prompt peaks in SEP event time profiles. Adv. Space Res. 39, 1882–1889. https://doi.org/10.1016/j.asr.2007.01.070.

Mäkelä, P., Gopalswamy, N., Akiyama, S., Xie, H., Yashiro, S., 2011. Energetic storm particle events in coronal mass ejection-driven shocks. J. Geophys. Res. (Space Phys.) 116, A08101. https://doi.org/10.1029/2011JA016683.

Rao, U.R., McCracken, K.G., Bukata, R.B., 1967. Cosmic ray propagation processes 2: The energetic storm-particle event. J. Geophys. Res. 72, 4325–4341. https://doi.org/10.1029/JZ072i017p04325.

Reames, V.D., 1999. Solar energetic particles: Is there time to hide? Radiat. Meas. 30, 297–308. https://doi.org/10.1016/S1350-4487(99)00066-9.

Reames, V.D., 2004. Solar energetic particle variations. Adv. Space Res. 34, 381–390. https://doi.org/10.1016/j.asr.2003.02.046.

Reames, V.D., 2012. Particle energy spectra at travelling interplanetary shock waves. Astrophys J 757, 93. https://doi.org/10.1088/0004-637X/757/1/93.

Turner, R., 2001. What we must know about solar particle events to reduce the risk to astronauts. Washington DC American Geophysical Union Geophysical Monograph Series 125, 39–44. https://doi.org/10.1029/GM125p0039.

Wijsen, N., Aran, A., Scolini, C., et al., 2022. Observation-based modelling of the energetic storm particle event of 14 July 2012. Astron. Astrophys. 659, A187. https://doi.org/10.1051/0004-6361/202142698.

Vršnak, B., Žic, T., Falkenberg, T., et al., 2010. The role of aerodynamic drag in propagation of interplanetary coronal mass ejections. Astron. Astrophys. 512, A43. https://doi.org/10.1051/0004-6361/200913482.

Vršnak, B., Žic, T., Vrbanec, D., et al., 2013. Propagation of interplanetary coronal mass ejections: The drag-based model. Sol. Phys. 285, 295–315. https://doi.org/10.1007/s11207-012-0035-4.

Xie, H., Ofman, L., Lawrence, G., 2004. Cone model for halo CMEs: Application to space weather forecasting. J. Geophys. Res. (Space Phys.) 109, A03109. https://doi.org/10.1029/2003JA010226.